Astron. Astrophys. 338, 737–746 (1998)

ASTRONOMY AND ASTROPHYSICS

Generation of solar Hα impact polarization by fragmented evaporative upflows

L. Fletcher and J.C. Brown

Department of Physics and Astronomy, University of Glasgow, Glasgow G12 8QT, UK

Received 13 December 1995 / Accepted 3 June 1998

Abstract. In this paper a novel mechanism is proposed for the generation of Hα impact polarization observed during some solar flares. Rather than being generated by the primary particle beams transporting energy from the chromosphere to the corona, we suggest that following heating, the solar chromosphere evaporates in a fragmented manner, and that impact excitations in the regions of interaction of hot evaporating and cool non-evaporating material locally generates impact-polarized Hα emission. This thermal upflow model is more consistent with the large areas and times over which polarization is observed than are beam models. A simple model for the process is given, and the resulting polarization is calculated and compared with observations, under two assumptions about the number density of neutral particles in the interaction regions.

Key words: Sun: flares – Sun: chromosphere – polarization

1. Introduction

Treatments of the generation of polarized Hα emission in solar flares have thus far concentrated on its interpretation in terms of excitation by a high-energy particle beam, moving from the corona to the chromosphere during the initial energy release phase of the flare (e.g. Hénoux et al. 1990, Hénoux 1991, Fletcher & Brown 1995, Karlický et al. 1996) or by an electron distribution carrying a heat flux, also moving from chromosphere to corona. (Hénoux et al. 1983, Aboudarham et al. 1992). However, we propose that excitation by flows moving *upwards* from the chromosphere to the corona is also a feasible mechanism. Such upward flows are thought to occur during and after the impulsive phase of solar flares, when the atmosphere, which has been greatly heated by various processes, including particle beams during the energy release phase, can undergo upward hydrodynamic expansion (evaporation). Observational evidence for this expansion, with velocities of a few 100 km s^{-1} has been presented (e.g., Antonucci et al. 1990 a,b) in the form of blue-shifts in certain chromospheric and transition region soft X-ray lines, which have been modeled by emission from multi-thermal plasma with a range of velocities (Alexander 1990), or from one or two discrete plasma components. An evaporating proton of $v = 100\mathrm{kms}^{-1}$ ($E = 50$eV) colliding with a neutral hydrogen atom has more than enough kinetic energy to excite a ground-state atom to level 3, from which decay to level 2 results in the emission of Hα radiation. The threshold for excitation to level 3 is 12.09 eV from level 1, and 1.89 eV from level 2.

There are several factors which prompt investigation of a gradual phase evaporative mechanism for excitation of Hα impact polarization. In the majority of flares in which it is observed, Hα polarization occurs during the rise of SXR emission, associated with the flare atmospheric response, without any HXR counterpart. It is present over a large area - up to a few times 10^{19} cm^2, comparable to the areas over which blueshifted Hα brightenings (indicating heating and acceleration) are observed to occur (Antonucci et al. 1990b), but much larger than the chromospheric area of impulsive beam, typically a few times 10^{17} cm^2, inferred from Yohkoh HXR images (e.g. Masuda 1994). Polarization remains at a high level for a considerable period of time - as long as 30 minutes in some cases, although more usually the duration is 10 - 15 minutes, again comparable to the timescales of 10 minutes, during which Antonucci et al. observe evaporation at 100 km s^{-1}. The flare impulsive phase lasts typically less than 5 minutes. These facts are all consistent with the polarization being part of the gradual phase atmospheric response to the flare energy input (though there is an example (Metcalf et al. 1992) of a smaller, shorter duration flare in which time profiles of impulsive hard X-rays and Hα polarization tracked one another, suggesting an impulsive phase origin for the polarization.)

An evaporative model.

The requirements for the generation of Hα impact polarization are simple. There must be neutral hydrogen, an anisotropic distribution of exciter particles with energy at least equal to the level 3 excitation energy, and a region in which the two populations interact. All three conditions can be fulfilled by a model in which evaporation, with a velocity $\gtrsim 100\mathrm{kms}^{-1}$ or above, takes place in discrete channels, through a static atmosphere (see Fig. 1). The fragmented evaporation channels leave the surrounding material relatively undisturbed, and it is in the region between the channels and the surroundings that excitation of the neutral

Send offprint requests to: L. Fletcher: from 1 May 1998 at Lockheed-Martin Solar and Astrophysics Laboratory, Dept. H1-12, Building 252, 3251 Hanover St., Palo Alto, CA 94304, USA (fletcher@sag.lmsal.com)

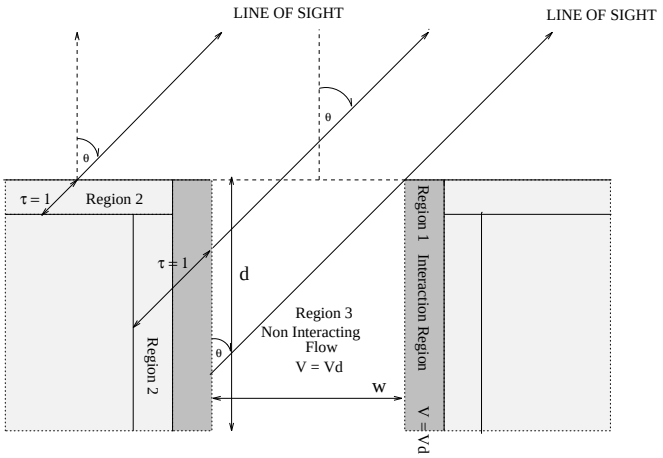

Fig. 1. Diagram of the interaction region (region 1), the static surroundings which are visible in Hα (2,2a) and the ionised flow (3).

hydrogen takes place. A large number of channels is needed to give a sufficient visible area for this boundary interaction region. The surroundings containing the neutral hydrogen target, have density and temperature given in flare model atmosphere F1 of Machado et al. (1980).

The evaporating material is assumed to be isothermal, fully ionised hydrogen. We look at flow temperatures of 10^5 to 10^7 K, and densities of $10^{10} - 10^{11}$ cm^{-3}, in accordance with the values found numerically by Nagai & Emslie (1983) in their hydrodynamic simulations of evaporation following impulsive electron-beam heating, and by Hénoux & Karlický (1994) in their hybrid treatment of beam transport and evaporation.

In the remainder of the paper we explore this model for the generation of polarized Hα radiation. In Sect. 2 we describe the sources of polarized and unpolarized radiation from the upflowing region, the atomic data and the calculation of flow anisotropy factors. Two cases are then studied, each with a different assumption about the number density of neutral particles in the interaction region. Results for these are presented in Sects. 3 and 4. Our discussion and conclusions are presented in Sect. 5.

2. Emission from the flow channels

The section marked 'interaction region' (region 1) in Fig. 1 is where polarized radiation would originate. It is the transition between hot flow and cool stationary material. The flow material is moving upwards with a velocity $\gtrsim 100$kms^{-1} whilst the non-flow material is static. The flow material, being ionised, is constrained to move along the solar magnetic field which is assumed to be locally vertical in the chromosphere. It therefore cannot penetrate any more than a Larmor radius into the surrounding non-flow material. However, neutral hydrogen in the surroundings is not constrained to vertical motion and is free to diffuse across the field and enter the ionised flow. When it does so it will be excited and emit impact radiation.

Of course, neutral material cannot completely interpenetrate the ionised flow - it will itself eventually become ionised by collisions, or charge exchange, and be swept up with flow material. The distance r_i by which the neutral gas penetrates is equal to its transverse (thermal) velocity multiplied by the time taken for ionisation or charge exchange, whichever is smaller. This time is $\tau = (n_f v_p \sigma)^{-1}$, n_f being the flow proton number density, and v_p the flow proton speed. The important collision process is that which has the larger cross-section σ at the typical energies with which flow protons and diffusing non-flow hydrogen collide i.e ~ 100eV. At energies less than 40keV the charge - exchange cross section σ_c is larger (c.f. Mott & Massey 1965, Lüdde & Dreizler 1982). At low energy, σ_c decreases with decreasing energy towards the lowest energy value calculated at 1keV (Lüdde & Dreizler). Here $\sigma_c = 1.47 \times 10^{-15}$cm^2. We may expect that σ_c will continue to decrease towards zero, so we use 1.47×10^{-15}cm^2 as an upper limit to σ_c at 100eV giving a lower limit to the interpenetration distance. Using a flow density of 10^{10}cm^{-3}, and proton speed equal to a high drift speed of 10^8 cm s^{-1} gives $\tau = 6.8 \times 10^{-4}$s, so a neutral hydrogen atom with thermal speed of 1.5×10^6cm s^{-1} (corresponding to a temperature of the surrounding material of T $\sim 10^4$ K) has interpenetration distance ~ 1000 cm. At a flow speed of 10^7cm s^{-1} and density of 10^{10}cm^{-3} the interpenetration distance is $\sim 10^4$cm.

We consider the case of narrow upflows, such that the radius of the upflow is comparable to the interpenetration distance, and essentially all of the upflowing area is emitting polarized radiation. These upflows correspond to features smaller than can be resolved, but there is theoretical evidence that such narrow structures can exist (see Sect. 5). The net polarization from the entire surface is then the undiluted polarization fraction from the interacting regions, diluted by emission from flow and surroundings.

2.1. Hα emission from the interaction region

In the interaction region (1) diffusing neutral hydrogen is excited by collisions with flow electrons and protons. We assume that the flow is a drifting Maxwellian distribution, with local temperature T and upward drift speed v_d. It thus has a bulk speed v_d, on which is superimposed isotropic thermal motion appropriate to the flow temperature. The diffusing neutral particles, which are being excited, are assumed to have zero velocity in the rest-frame of the solar chromosphere. (In fact they have a randomly directed diffusion speed of $\sim 10^6$cm s^{-1} - the mean thermal speed for hydrogen in the static surroundings - but this is small compared to the upflow speeds of $10^7 - 10^8$cms^{-1}.)

The polarization of photons emitted depends on the anisotropy of the 'exciter' distribution which depends on the ratio between drift speed and mean thermal speed - the larger the ratio, the larger the anisotropy (and the larger the polarization fraction.) We consider flows with temperatures between 10^5 and 10^7 K, so the flow electron mean thermal speed (in the rest-frame of the flow) is $2 \times 10^8 - 2 \times 10^9$ cms^{-1} (large compared to typical flow sppeds) and the flow proton mean thermal speed is $5 \times 10^6 - 5 \times 10^7$ cms^{-1}. The proton component will therefore be the more anisotropic of the two, and we shall calculate

polarization arising only from it. Of course flow electrons also collisionally excite Hα in the interaction region, but we assume this to be unpolarized (though in reality it is polarized, with the same sign as that generated by the protons) and, along with collisional and recombination emission from the surroundings, it will dilute the proton-excited polarized radiation.

The flow electron generated collisional Hα intensity, I_e, in the interaction region can be approximately calculated as the emission from a Maxwellian $f(v_e, T)$, of temperature equal to the flow electron temperature, exciting a population n_i in the i'th excitation state of neutral hydrogen, ie.

$$I_e = n_e n_i \int_{v_{th}}^{\infty} f(v_e, T)\sigma_{e,i-3}(v_e)v'_e dv_e \quad \text{photons /s/cm}^{-3}. \quad (1)$$

The density of flow electrons in the interaction region is $n_e = n_p = n_f$. The density n_i of level i hydrogen should be calculated from the balance between emission and excitation in the region, but in practise we consider two cases. In the first, case A (Sect. 3), we assume that the populations of level 1 and level 2 neutral hydrogen in the interaction region are given by the F1 model values. In the second, case B, we postulate that the level 1 population is given by the F1 value, but calculate the population of level 2 by considering the rate equations (Sect. 4).

The electron excitation cross section for Hα, $\sigma_{e,i-3}(v_e)$ at the relevant (high) thermal speeds, is calculated in the Born approximation, from Vainshtein (1965), matched at the low speeds to the measurements of Mahan et al. (1976) (cf. Fletcher & Brown 1995). A second term of the same form as Eq. 1 describes the excitation from level 2 to 3 with the cross sections coming from Omidvar (1963)

Because of the addition of a bulk flow speed comparable to the thermal proton speed, the proton flow becomes significantly non-Maxwellian and anisotropic in the rest-frame of the surrounding neutrals. The flow-proton generated emission is given by

$$I_p = n_p n_i \int_{v'_p} J_0(v'_p)v'_p\sigma_{i-3}(v'_p)dv'_p \quad \text{photons /s/cm}^{-3}, \quad (2)$$

where v'_p is the proton velocity in the rest frame of the particles being excited (see Eq. 6). Here J_0 is the zeroth moment of the proton distribution function. We calculate level 1-3 and level 2-3 excitations. Theoretical proton excitation cross-sections at a minimum proton excitation energy of 1keV are presented by Lüdde & Dreizler (1982) for the 1s - 3 transition, and by Khandelwal & Choi (1968) for the 2s - 3 and 2p - 3 transitions. In some cases, the energy of the protons we consider is less than 1keV, depending on the flow speed, and for these cases we assume that the cross-sections vary linearly with energy from 1keV down to zero at threshold.

At low proton energy, neither experimental data nor theoretical calculations of polarization fractions are available so we must resort either to electron data or theoretical arguments. Percival & Seaton (1958) argued that at threshold excitation energy, the exciting particle must come out of the collision with zero energy and therefore zero angular momentum. The total angular momentum of the upper state excited in this transition must then be equal to the total angular momentum of the level from which excitation occurred. Therefore, not all spin and orbital sub-levels can be excited at threshold. This limitation allows the calculation of a theoretical threshold polarization fraction. The three downwards transitions contributing to the Hα line are 3s-2p, 3p-2s and 3d-2p. Syms et al. (1975) find that, following threshold excitation from an $l = 0$ state (1s or 2s), an $l = 1$ to $l = 0$ downwards transition (ie., 3p-2s) yields a polarization fraction of 43%, and an l=2 to l=1 transition (ie., 3d-2p) yields 48%. The 3s-2p transition is unpolarized. Polarization is highest if single upper quantum states are excited, but the ratio in which the upper states are excited is dependent on the populations of the lower levels, and the cross-sections near threshold, which are not known for protons. We take an upper limit to the polarization fraction of 43%, this high value being equivalent to saying that de-excitation from one particular upper angular momentum state dominates. Various effects can decrease this polarization fraction. Depending on the populations of the lower levels, more than one combination of spin and orbital angular momentum substates can be excited, even at threshold, and in general the excitation of more than one upper state will lead to smaller polarizations. The polarization should decrease as the energy of the exciting particle increases away from threshold (this again increases the number of upper states which can be excited) - electron data just above threshold gives a value of $\sim 30\%$ (Syms et al. 1975) though low energy resonance effects between test proton and hydrogen target may change this. We have neglected fine-structure splitting in our calculations. Vogt et al. (1997) have calculated its effect and find a depolarization of up to an order of magnitude. All these depolarizing effects can be countered by increasing the number flux of exciter particles.

Finally the polarization generated by the anisotropic proton distribution function is given by

$$P_{90} = \frac{3J_2 - J_0}{2} P_{beam}(v_d, T) = b(v_d, T)P_{beam}(v_d, T). \quad (3)$$

where J_2 is the second moment of the proton distribution function and $b(v_d, T)$ is the proton 'anisotropy factor' (Hénoux et al. 1983). This factor gives a measure of how isotropic the electron distribution is for the purposes of calculating impact polarization - for a completely isotropic distribution $b = 0$, whilst for a beam distribution $b = 1$. The form shown above is derived from the expressions for the Stokes' Q and I parameters for a cylindrically symmetric exciter distribution (Hénoux et al. 1983). P_{90} is the polarization obtained from a distribution with anisotropy factor $b(v_d, T)$ under conditions where a completely unidirectional beam of speed v_d would generate P_{beam}, when viewed at $90°$. If one observes at an angle θ to the direction of travel of the flow (i.e., the local solar vertical direction) the polarization fraction is reduced to

$$P(\theta) = P_{90} \sin^2\theta/(1 - P_{90}\cos^2\theta). \quad (4)$$

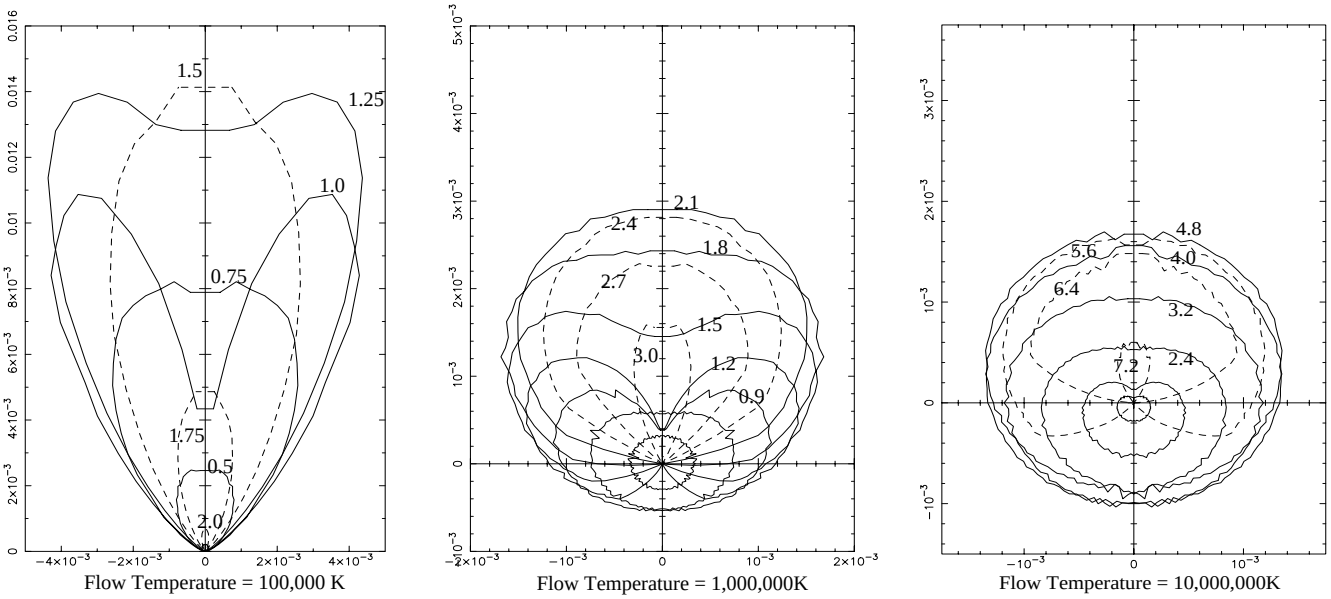

Fig. 2. Polar diagram of flow particle distributions of speeds. The drift velocity is 10^7 cm s^{-1} and the numbers on the contours are the particle speeds in units of 10^7 cm s^{-1}. Solid and dashed lines are merely an aid to distinguishing the various contours. The axes are numbered in scaled values of the electron number density in a particular direction. At a given point on a particular curve the (scaled) value of the density is $\sqrt{(x_o^2 + y_o^2)}$ where x_o, y_o are the x, y- co-ordinates of the point.

2.2. Moments and anisotropy factor of the flow protons

The moments of the flow in the rest-frame of the static chromosphere are described by

$$J_n(v') = \int_{-1}^{1} \mu'^n f(\mu', v') d\mu' \tag{5}$$

where μ' is the particle pitch angle cosine. In the rest frame of the flow the particle distribution is the isotropic Maxwellian distribution If we add a drift speed v_d to the z-velocity component of a typical flow proton then, as viewed from the rest-frame of the static chromosphere, a flow proton which in the rest frame of the flow had co-ordinates (v, μ) now has co-ordinates (v', μ'). These are related by

$$v^2 = v'^2 + v_d^2 - 2v'v_d\mu'. \tag{6}$$

In the flow rest-frame the number of particles dn in a small interval $\delta v \delta\mu \delta\phi$ around (v, μ) is proportional to the value of the Maxwellian distribution function at that velocity multiplied by the volume of the interval. Under the z-transformation to the chromospheric rest frame the dn particles end up in transformed interval $\delta v' \delta\mu' \delta\phi$. The stationary Maxwellian is evaluated in 300 pitch angle intervals covering the range $0 - 180°$, and the speed in 200 intervals covering zero to a few times the thermal speed. The number of particles at (v, μ) is then assigned to the new position (v', μ') in the shifted distribution and rebinned into broader speed and pitch angle bins. The results of these transformations in the form of polar diagrams of the flow distributions viewed from the static chromosphere rest frame are shown in Fig. 2. An analytic approach to this problem is to be found in Laming (1990).

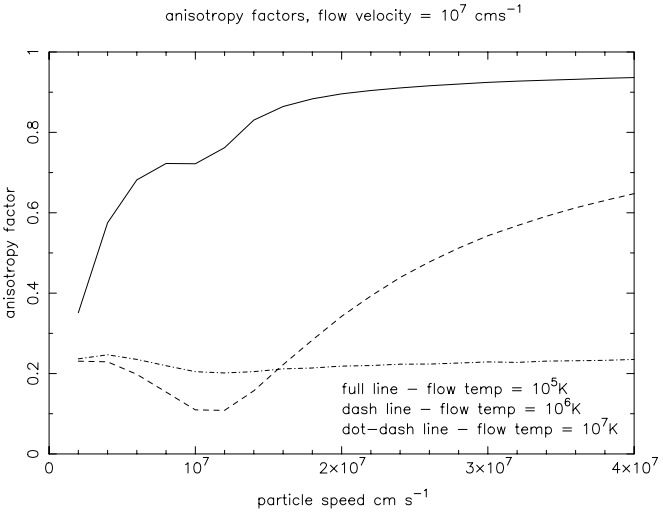

Fig. 3. Anisotropy factors for the flows of Fig. 2.

To calculate the functional moments, integral (5) is evaluated. We only have values for the distribution function at discrete, evenly spaced values of v' and θ' so we use a trapezoidal rule to approximate the integral. The results of these calculations are used to find the anisotropy factor of the distribution as a function of v', which is plotted in Fig. 3 for various values of the flow temperature, at a flow speed $v_d = 10^7$cm s^{-1}. Anisotropy factors become higher for higher values of v_d. It can be seen that, in general, lower temperature (lower thermal velocity) distributions have, as expected, a higher anisotropy factor at a given v'.

3. The polarization fraction - case A

We first present a calculation of the polarization fraction in the case that the number densities of the target neutrals in the interpenetration region is equal to their values in the F1 model chromosphere. In Table 1 we present results of the calculation of the polarization fraction of Hα emission by the interacting material *alone*, for selected values of flow temperature and drift speed. The first row is $b(v_d, T)P_{beam}$, the proton-excited, undiluted polarization fraction viewed at 90° to the flow direction. The second row is the maximum value of the ratio of intensity of emission excited by the proton component of the flow (which is polarized) to that excited by flow electrons (assumed unpolarized) and protons combined. An upper limit to the net polarization fraction of radiation, resulting solely from collisions in the interaction region viewed at 90° to the flow direction, is given in row 3.

The polarization fractions can be up to 5%, indicating that the ratio of polarized flow-proton emission to unpolarized, flow-electron generated emission is quite high. Because of the larger excitation cross-section, the electrons dominate the 1-3 transition, but the proton cross-section for excitation of the 2-3 transition is approximately ten times that for electrons. Therefore the protons still contribute significantly overall. Note that the polarization fractions given here have yet to be diluted by the unpolarized emission from the surrounding material, as calculated in the following sections.

3.1. Hα emission from the surroundings

'The surroundings' are the static chromosphere (region 2 in Fig. 1) and the non-interacting flow (region 3). The static chromosphere emits both collisional and recombination Hα. The collisional intensity is given by an equation of the form of (1), using now electron densities and temperatures taken from the Machado et al. (1980) F1 model. The recombination intensity is

$$I_r(z) = 8.8 \times 10^{-7} n_p n_e T^{-1.5} exp\left(\frac{\chi_3}{kT}\right) E_i\left(\frac{\chi_3}{kT}\right) \qquad (7)$$

photons s^{-1} cm^{-3}, where χ_3 is the ionisation potential of level 3 and E_i is the exponential integral function. The surface flux from the static chromosphere, F_{stat}, found by numerically integrating the emission, taking into account the variation in optical depth (see Sect. 3.2) can be calculated for an arbitrary angle θ to the vertical. When viewed along the local vertical, $F_{stat} \sim 1.6 \times 10^{17}$ photons $cm^{-2}s^{-1}$.

Though we assume that the flow channel radius is comparable to the interpenetration distance, in which case there may be no non-interacting flow, we discuss briefly its optical properties. The non-interacting flow is assumed to be completely ionised, so non-absorbing, and it also emits only recombination emission. At a temperature of 10^5 K the emission from the non-interacting flow region is $\lesssim 5.95 \times 10^7$photons $cm^{-3}s^{-1}$ and at 10^7K it is $\lesssim 2.20 \times 10^5$ photons $cm^{-3}s^{-1}$. This can be neglected in comparison with the typical static chromosphere thermal emission of $\sim 10^{11}$photons $cm^{-3}s^{-1}$. Further, the low density of the non-interacting flow means in that Thompson scattering of radiation can be neglected.

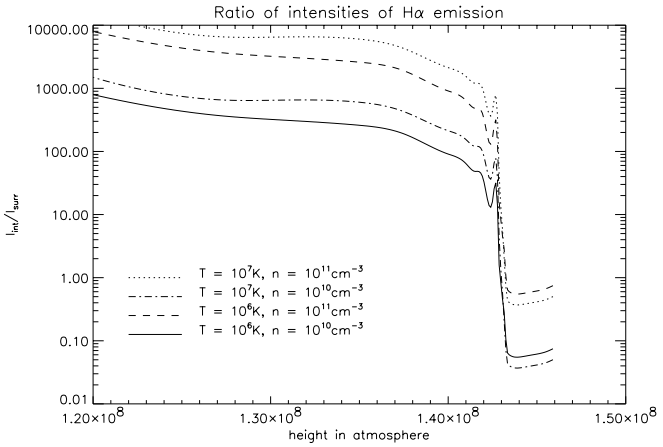

Fig. 4. The ratio of Hα intensity generated in the interaction region to that generated in the static chromosphere, as a function of position. The plot is made for a flow speed of 5×10^7cm s^{-1}. This is for case A - the number density of neutral particles in the interaction region is equal to the F1 values.

In Fig. 4 we plot the ratio of Hα intensity in the interaction region to that in the surroundings, as a function of position in the chromosphere, for a variety of flow temperatures and densities, at a flow speed of 5×10^7cm s^{-1}. Note that the positions are measured upwards from the $\tau_{5000} = 1$ level, the nominal base of the chromosphere. The high value of this ratio below about 1.4×10^8 cm is due to the high excitation rates (because of high flow temperature and density) in the interaction region, compared to that in the surrounding F1 model atmosphere. However, this region is optically thick to Hα. The slow, then rapid, decrease in the ratio with increasing height is due to the increase in the temperature of the surroundings whilst the flow temperature remains constant. The dip between 1.42 and 1.43×10^8cm is at the location where collisional Hα excitation is at a maximum in the surrounding F1 atmosphere (at the position of maximum $n_e \times n_1$). The slow rise above 1.44×10^8cm occurs because the number density of electrons and protons causing the collisional excitation is assumed constant with height in the flow, but decreases with increasing height in the surrounding atmosphere. However, Fig. 4 hides the fact that above 1.43×10^8 cm the Hα emission from both flow and surroundings drops to very low levels.

3.2. Hα absorption

We calculate the total flux at the surface by integrating the intensity as a function of depth along the line-of-sight, taking into account the increasing optical depth along the path, so the contribution from position l_o is diluted by $e^{-\tau(l_o)}$. We assume that absorption in the Hα line is line centre absorption in a Doppler

Table 1. Polarization from interaction material - case A

	Temperature = 10^6K			Temperature = 10^7K		
Velocity (cms^{-1})	10^7	5×10^7	10^8	10^7	5×10^7	10^8
$b_(v_d)P_{beam}$	25.5%	40.7%	41.5%	13.3%	31.0%	37.0%
$I_{prot}/I_{elec}+I_{prot}$	7×10^{-4}	0.065	0.12	0.001	0.095	0.17
Net Polarization (90°)	0.02%	2.7%	5.0 %	0.01%	2.9%	6.3%

broadened line. The optical thickness in the line centre along a path l_o is given by the following expression

$$\tau(l_o)=\int_{l_o}\alpha n_2(l)dl \tag{8}$$

where n_2 is the level 2 hydrogen number density and α is the line centre absorption coefficient for the Hα line, wavelength λ_{3-2}, given by

$$\alpha=\frac{3\lambda_{3-2}^3}{8\pi}\left(\frac{m_h}{2\pi kT(l)}\right)^{\frac{1}{2}}A_{3-2}\sim\frac{6.5\times10^{-11}}{\sqrt{T(l)}}\quad\mathrm{cm}^2. \tag{9}$$

A_{3-2} is the Einstein A coefficient for the 3-2 transition. In this geometry, any line-of-sight encompasses a large number of narrow flow channels and intervening static atmosphere. We therefore use the following expression for the average optical depth along path l_o

$$\tau(l_o)=\int_{l_o}f\alpha_{stat}n_{2,stat}(l)+(1-f)\alpha_{up}n_{2,up}(l)dl, \tag{10}$$

where f is the volume filling factor of the channels (=surface filling factor for vertical channels) and the subscripts refer to the static and interacting upflowing material. In case A the temperature and the density of the level 2 hydrogen atoms in the interpenetration region and the surroundings are from the Machado et al. F1 model atmosphere.

Though some account is taken of the absorption of Hα, this does not in any way constitute a full treatment of the transfer of polarized radiation. It is assumed that the polarization fraction remains unchanged over a photon's path. In fact this may not be too poor an assumption as it turns out that, because of the rapid increase in the n_2 population in both the interaction region and the surrounding chromosphere, the atmosphere can be considered as varying from optically thin ($\tau<0.01$) to optically thick ($\tau>10$) over a very short distance. This change takes place at $\sim1.42-1.43\times10^8$cm above the base of the chromosphere, depending on the viewing angle. Photons generated below this boundary are absorbed and photons emitted above this boundary travel through practically optically thin material.

3.3. The net polarization

If the surface flux from the upflowing region is $F_{up}(\theta)$ and that from the static surroundings is $F_{stat}(\theta)$ with the filling factor of the flow channels being f, then the net polarization is

$$P_{net}=\frac{P(\theta)F_{up}(\theta)}{fF_{up}(\theta)+(1-f)F_{stat}(\theta)} \tag{11}$$

(assuming that the interpenetration distance is equal to the upflow radius) where $P(\theta)$ is the polarization fraction adjusted for dilution by electron emission in the interacting region. The surface flux is obtained by integrating up the contributions from all elements along a line of sight, between the top of the chromosphere and the position $\tau=1$. (An example of the surface flux ratio for case B is shown in Fig. 8 - ratios obtained for case A are not shown here.) The resulting net polarization fraction from the various models is shown in Fig. 5.

The 1 % level is obtained for viewing angles to the vertical between 20 and 55° degrees. At present all published observations lie within this range. At small viewing angles, $\sin\theta$ tends to 0 in Eq. 4. At large angles, the ratio of surface fluxes from interacting and static material decreases, for the following reason: as one views at progressively greater angles to the local vertical, the vertical distance, measured from the top of the atmosphere, down to the position $\tau=1$ decreases - one only sees emission from these higher layers. As is shown in Fig. 4, emission from the interaction region is a smaller fraction of the total in the upper layers of the atmosphere (excepting heights $\gtrsim1.44\times10^8$cm (where Hα emission is at a negligible level anyway).

4. The polarization fraction - case B

We turn now to the case in which the number density of level 1 hydrogen in the interaction region is taken to be equal to its F1 value, but the level 2 density is calculated by looking at the various collisional and radiative processes happening in this region. Level populations should be calculated by solving the rate equations for all hydrogen levels, including radiative and collisional excitation and de-excitation, but such a calculation is outwith the scope of this paper - we do a rate calculation for level 2 in isolation. Below is a list of the population and de-population rates and the expressions with which they are evaluated. Note that we have here assumed that the Lyman α line (the 2-1 transition) is in detailed radiative balance (radiative excitation and spontaneous de-excitation cancel) in line with, e.g. Brown et al.'s 1978 work on beam excitation of Hα radiation. It is reasonable to assume

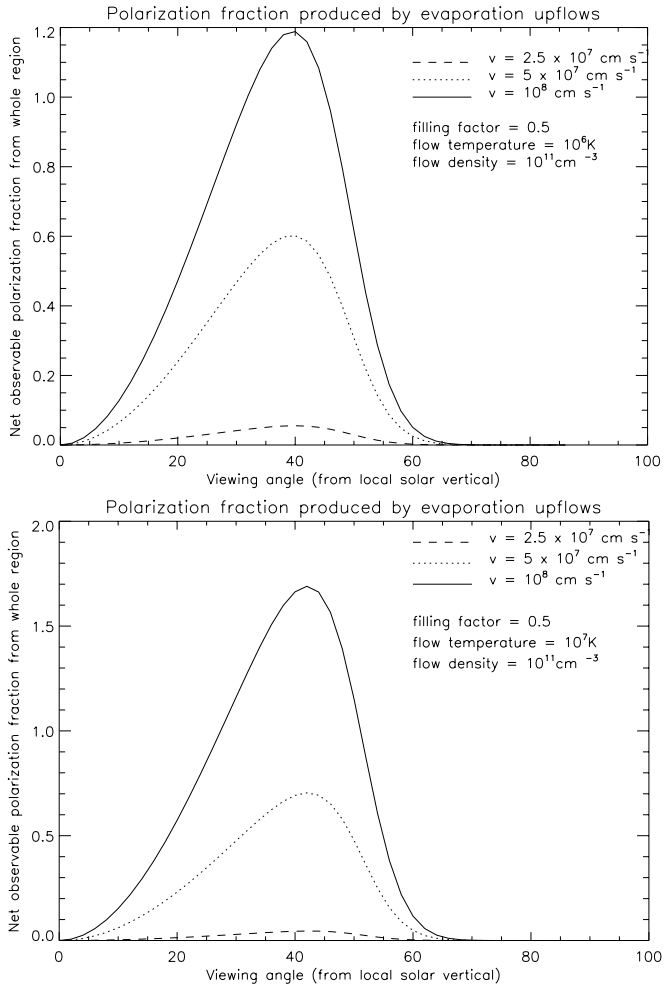

Fig. 5. Polarization fractions from narrow upflows for a variety of flow parameters, case A.

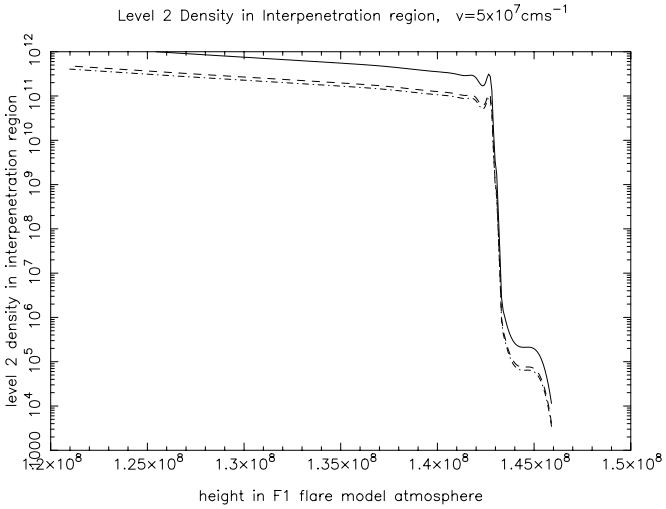

Fig. 6. Variation of level 2 density in the interaction region for three values of flow temperature and a flow density of 10^{10} protons cm s^{-1}. The full, dash and dot-dash lines correspond, respectively, to $T = 10^5, 10^6$ and 10^7K.

that such balance can exist: the column depth of n_1 for which $\tau = 1$ in the Lyman α line is a few times $\sim 10^{13}\mathrm{cm}^{-2}$ at 10^4 K (assuming line - centre absorption in a Doppler-broadened line) which is comparable to the transverse level 1 column depth of the interaction region ($\sim 10^{10}\mathrm{cm}^{-3} \times 10^3\mathrm{cm}$).

Level 2 populating processes operating in the interaction region

1) Excitation of level 1 hydrogen by flow electrons.
$n_1 n_e \int v_e \sigma_{1\rightarrow 2}(v_e) f_e(v_e) dv_e$
for $\frac{1}{2} m_e v_e^2 > E_{1-2}$
2) Excitation of level 1 hydrogen by flow protons.
$n_1 n_p \int v'_p \sigma_{1\rightarrow 2}(v'_p) J_0(v'_p) dv'_p$
3) Spontaneous de-excitation from level 3 and above (e.g. Hα emission).
$\Sigma_{j=3}^{\infty} n_j A_{j,2}$
We only consider de-excitation from level 3 (Machado et al. model does not give data on level 4 populations).
4) Recombination of flow electrons and protons to level 2.
$n_e n_p \alpha_2$
α_2 is the recombination coefficient to level 2.

5) Drift of level 2 particles in from the ambient plasma.
$n_2 v_{th,2}$
$v_{th,2}$ is the mean thermal speed of level 2 particles from the static chromosphere.

Level 2 depopulating processes operating in the interaction region

6) Collisional excitation up from level 2, by flow electrons
$n_1 n_e \int v_e \Sigma_{j=2}^{\infty} \sigma_{2\rightarrow j}(v_e) f_e(v_e) dv_e$
We consider only the 2-3, 2-4 and 2-5 excitations.
7) Collisional excitation up level 2, by flow protons.
$n_1 n_p \int v_p \Sigma_{j=2}^{\infty} \sigma_{2\rightarrow j}(v_p) J_0(v_p) dv_p$

Balancing these excitation and de - excitation terms leads to an equation for n_2 in the interaction region. Fig. 6 shows the variation of level 2 density with position in the interaction region.

The populations are shown for three different flow temperatures, at a flow speed of $v_d = 5 \times 10^7 \mathrm{cms}^{-1}$ and a flow density of 10^{10}protons cm^{-3}. The increase in interaction region level 2 density with decreasing depth corresponds to the increase in the density of neutral hydrogen diffusing in from the surroundings (and being excited to level 2 by collisions with flow particles) deeper in the atmosphere. The n_2 values calculated in case B are higher than the F1 values by 2-5 orders of magnitude.

4.1. The undiluted polarization fraction of interaction material, and the net polarization fraction

We proceed with the calculation of polarization fraction as in Sects. 3.1 to 3.3, but using now the new values of level 2 hydrogen density. Table 2 presents results of the calculation of the polarization fraction of Hα emission by the interpenetrating material.

Table 2. Polarization from interaction material, case B.

	Temperature = 10^6K			Temperature = 10^7K		
Velocity (cms^{-1})	10^7	5×10^7	10^8	10^7	5×10^7	10^8
$b_(v_d)P_{beam}$	25.5%	40.7%	41.5%	13.3%	31.0%	37.0%
$I_{prot}/I_{elec}+I_{prot}$	0.01	0.39	0.56	0.01	0.50	0.66
Net Polarization (90°)	0.2%	15.9%	23.2%	0.1%	15.5%	24.4%

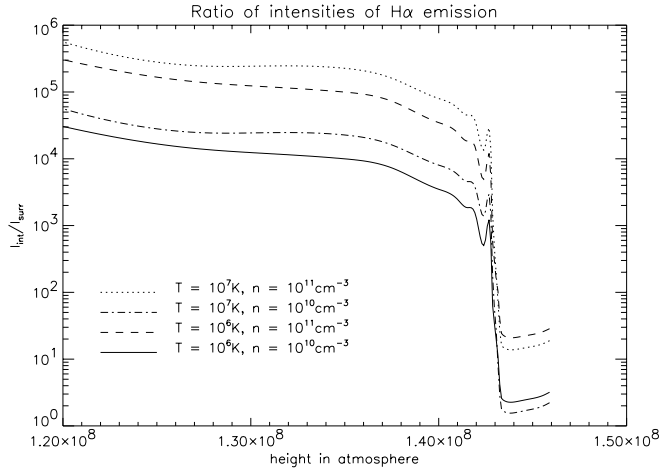

Fig. 7. The ratio of Hα intensity generated in the interaction region to that generated in the static chromosphere, as a function of position, case B. The plot is made for a flow speed of 5×10^7cm s^{-1}.

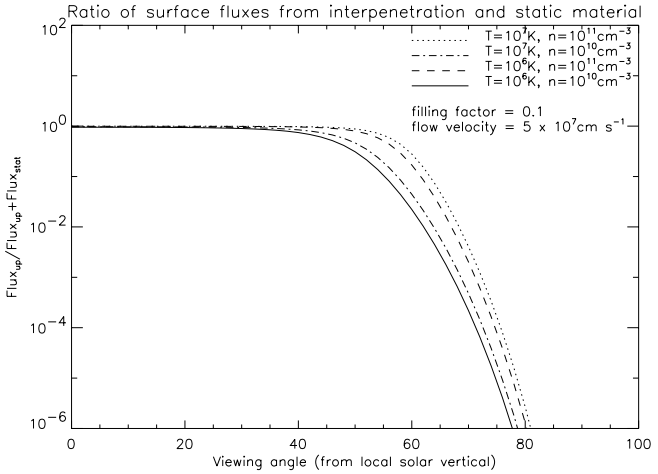

Fig. 8. The ratio of surface Hα flux in the interaction region to that from the static surface region, at $v_d = 5\times10^7\mathrm{cms}^{-1}$, case B.

In Fig. 7 we plot the ratio of Hα intensity in the interaction region to that in the surroundings, as a function of position in the chromosphere, for a variety of flow temperatures and densities, at a flow speed of 5×10^7cm s^{-1}. This looks very much like Fig. 4 except that the ratios are higher, accounted for by the higher level 2 populations.

In Fig. 8 we plot the ratio of surface flux from upflow regions to the total, for a flow speed of $v_d = 5\times10^7\mathrm{cms}^{-1}$, a filling factor for the upflows of $f = 0.1$, and a number of flow temperatures and densities, and the net polarization fraction from various parameter combinations, is shown in Fig. 9. The few % level is again obtained for viewing angles between 20° and 55°.

5. Discussion and conclusions

It has been shown that it is possible to generate impact polarization at the level of a few percent from the interaction of a filamented upward flow with a static surrounding atmosphere. We have studied two cases - the first where the number density of neutral particles being excited in the interaction region is equal to the number density in the F1 model atmosphere (implicit also in beam models where the effect of the beam on the population balance is neglected), and a second where the number density of level 2 particles is determined by a balance between excitation and de-excitation processes, in which the flow plays a part. This is similar to the approach taken by Vogt et al. (1997) who calculate level and sub-level populations in the atmosphere bombarded by a beam, including also the effects of radiative excitations.

The requirements on the flow are that it be fragmented into channels of radius 10^3-10^4cm, this being approximately equal to the interpenetration distance, which has as its lower limit the distance which a neutral hydrogen atom can penetrate the upflow before undergoing charge exchange. The filling factor of the upflows must be ~ 0.5. The temperature of the drift material must be 10^6-10^7 K with a drift velocity of a few times 10^7 cms $^{-1}$. There is observational evidence that upflows of this velocity occur on the sun during flares - Antonucci et al. (1990a,b) record evaporation velocities of 8×10^7 cm s^{-1} having a duration of ~ 5 minutes and a periodic time variation on a scale of 1.5 minutes (which is, incidentally, comparable to the time variation of the polarized area reported in Hénoux, 1991). In addition, theoretical work by Emslie & Alexander (1987) on the response of the chromosphere to heating by an electron beam suggests that upflow velocities of as much as 1.1×10^8 cm s^{-1} are possible in the low corona, if considering a multithermal plasma model of evaporation.

We must look at the energy flux in upflowing protons necessary to generate this emission. The average proton energy is $\sim$ 1 - 5keV, depending on flow speed and temperature. In case A, with a bulk speed of 5×10^7cm s^{-1}, and flow density of

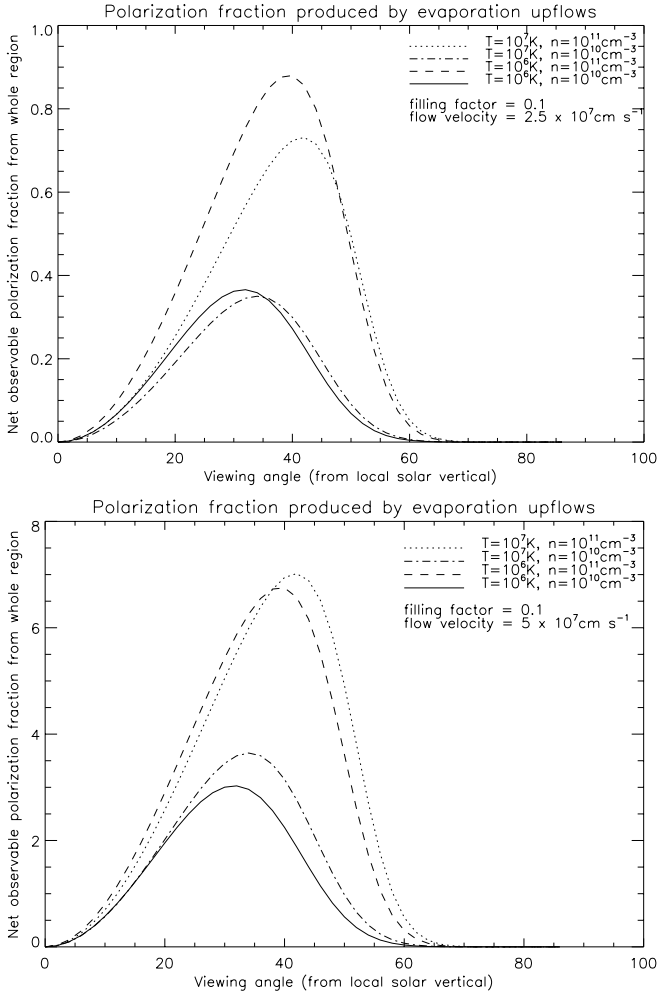

Fig. 9. Net polarization fractions for for a variety of flow parameters - case B.

$10^{11}\mathrm{cm}^{-3}$, the energy flux is 8×10^9 erg cm^{-2}s^{-1}. Using the flow filling-factor of 0.5 and an area of $10^{19}\mathrm{cm}^{-2}$ gives a total energy flux of $4\times10^{28}\mathrm{erg\,s}^{-1}$. Over the duration ($\sim 10^3$s) of the impact polarization observation, the typical total energy is only plausible for a large flare (with a total energy budget of $\sim 10^{32}$ erg). However, other authors (e.g. Vogt et al. 1997) take typical areas of $10^{18}\mathrm{cm}^{-2}$, which would put our total energy budget at 4×10^{30} erg, typical of a medium-sized flare. In case B, the flow density and filling factors can be lowered, and fluxes as low as $8 \times 10^{26}\mathrm{erg\,s}^{-1}$ are possible - well within the energy budget of a medium-size flare. In both cases there is some leeway for increasing the particle fluxes by up to an order of magnitude, to counter the depolarizing effects described in Sect. 2.

How might the finely filamented flows which we require arise and be sustained? A spatially fragmented evaporation could be driven by spatially fragmented energy release in the impulsive phase, and such processes have already been discussed in the literature. Holman (1985) pointed out that in the case of flare energy transport by electron beams generated in a single 'monolithic' accelerator, the best way to avoid disruption of the acceleration region by the return current produced by the large magnetic and electrostatic self-fields is to have the beam fragmented into a large number (at least 10^4) of oppositely directed current channels, meaning that the beam and return current are essentially co-spatial. Alternatively, the acceleration of flare particles in a spatially intermittent accelerator, possibly by many small reconnection events in a 'statistical flare' scenario, is increasingly being studied (e.g. Lu & Hamilton 1991, Vlahos et al., 1995, MacKinnon et al. 1996). One might expect that this type of acceleration onto a tangle of field lines could lead to energy being deposited over a large chromospheric area.

Such small scale structure can also persist outside the acceleration region. Gray & Brown (1996) calculate the maximum radius of filaments arising in an atmosphere heated in an arbitrary but spatially intermittent fashion, assuming that cross-field conduction in the chromosphere is the mechanism for removing heat from a heated core. The upper limit to the transverse scale of fragmentation is about $10^2 - 10^6$cm for chromospheric conditions (temperatures of $10^4 - 10^5$K and magnetic fields on the order of 100G) so on the scale of the narrow upflows which we consider.

In our calculations there are uncertainties which affect the net polarization values. The first of these is the uncertainty in atomic data regarding excitation by protons at low energies which may, as mentioned in Sect. 2.1, reduce the polarization values considerably. Resolution of this can only await suitable theoretical or experimental work. We have assumed that the electron component of the upflow does not produce any polarized radiation. This is not generally true. If the flow temperature is low but the flow speed is high, the electron component will also be anisotropic and generate polarized radiation, with a positive polarization vector, increasing the observed polarization.

A further shortcoming of this work is in our treatment of the transport of both polarized and un-polarized photons. Although our assumptions are in line with the level of complication of most previous work, the next sensible step in any work in this area is the treatment of the radiative transport of polarized radiation. In particular, a three-dimensional calculation of emission from interaction region is worthy of attention, especially in this case of highly fragmented structures, and is possible with Monte-Carlo treatments. Finally, in calculating the density of level 2 hydrogen in the interaction region in case B, we point out again that a full multi-level calculation of collisional and radiative excitation and de-excitation should be carried out. Calculations of the type performed by Vogt et al. (1997) may show the way.

Acknowledgements. L.F. is pleased to thank Jan Kuijpers of the Sterrekundig Instituut Utrecht, and J.C.Hénoux and an anonymous referee for improving previous versions of this paper. The authors further wish to acknowledge the support of PPARC grants and E.C. Lab-Twinning Contract SCI*-CT91-2027.

References

Alexander, D. 1990, A& A 235, 431

Aboudarham, J., Berrington, K., Callaway, J., et al. 1992, A& A 262, 302.

Antonucci, E., Dodero, M.A., Martin, R. 1990a, A& AS Ser. 73, 137.
Antonucci, E., Dodero, M.A., Martin, R. 1990b, A& AS Ser. 73, 147.
Brown, J.C., Canfield, R.C., Robertson,M.N. 1978, Sol.Phys. 57, 399.
Emslie, G.A. and Alexander, D., 1987, Sol. Phys. 110, 295
Fletcher, L., Brown, J.C. 1995, A&A 294, 260.
Gray, N., Brown, J. C. 1996, A&A 307, 955.
Hénoux, J.C., Heritschi, D., Chambe, G., et al. 1983, A& A 119, 223.
Hénoux, J.C., Chambe, G., Smith, D., et al. 1990, ApJS 73, 303.
Hénoux, J.C. 1991, In: L.November (ed) 'Solar Polarimetry', proceedings of the 11th NSO/SP Summer Workshop, New Mexico.
Hénoux, J.C., Karlický, M. 1994, A & A 283, 202.
Holman, G. 1985, ApJ 293, 584.
Khandelwal, G.A., Choi, B.-H. 1968, J.Phys.B 1, 1218.
Karlický, M., Hénoux, J. -C., Smith, D.F. 1996, A&A 310, 629.
Laming, J.M. 1990, ApJ 362, 219.
Lu, E. T. , Hamilton, R. J. 1991, ApJ 380, L89.
Lüdde, H.J., Dreizler, R.M. 1982, J.Phys.B 15, 2703.
Machado, M., Avrett, E.H., Vernazza, J.E., Noyes, R.W. 1980, ApJ 242, 336.
MacKinnon, A. L., Macpherson, K.P., Vlahos, L. 1996, A&A 310, L9
Mahan, A.H., Gallacher, A., Smith, S.J. 1976, Phys. Rev. A 13, 156.
Masuda, S. 1994, Ph.D. thesis, University of Tokyp
Metcalf, T., Wuesler, J.P., Canfield, R.C., Hudson, H.S. 1992, in proceedings of The Compton Observatory Science Workshop (SEE N92-21874 12-90), NASA/GSFC.
Mott, N.F., Massey, H.S.W. 1965, "The Theory of Atomic Collisions", Oxford University Press.
Nagai, F., Emslie, A.G. 1983, ApJ 279, 898.
Omidvar, K. 1963, Phys.Rev. 140, A38.
Percival, I.C., Seaton, M.J. 1958, Phil.Trans.Roy.Soc. 251, 113.
Syms, R.F., McDowell, M.R., Morgan, L.A., Myerscough V.P. 1975, J.Phys.B. 8, 2817.
Vainshtein, L.A. 1965, Opt. Spectrosc.(USSR) 11, 163.
Vlahos, L., Georgoulis, M., Kluiving, R., Paschos, P. 1995, A&A 299, 897.
Vogt, E., Sahal-Bréchot, S., Hénoux, J. -C. 1997, A&A 324, 1211.